JB
Journals.ASM.org

Insights into the Function of YciM, a Heat Shock Membrane Protein Required To Maintain Envelope Integrity in *Escherichia coli*

Valérie Nicolaes,[a,b,c] Hayat El Hajjaji,[a,c] Rebecca M. Davis,[d] Charles Van der Henst,[a,b,e] Matthieu Depuydt,[a,c] Pauline Leverrier,[a,c] Abram Aertsen,[f] Vincent Haufroid,[g] Sandrine Ollagnier de Choudens,[h] Xavier De Bolle,[e] Natividad Ruiz,[d] Jean-Francois Collet[a,b,c]

de Duve Institute, Université Catholique de Louvain, Brussels, Belgium[a]; WELBIO, Brussels, Belgium[b]; Brussels Center for Redox Biology, Brussels, Belgium[c]; Department of Microbiology, Ohio State University, Columbus, Ohio, USA[d]; University of Namur, Research Unit in Biology of Microorganisms, Namur, Belgium[e]; Laboratory of Food Microbiology, Department of Microbial and Molecular Systems, Faculty of Bioscience Engineering, Katholieke Universiteit Leuven, Leuven, Belgium[f]; Louvain Center for Toxicology and Applied Pharmacology, Institut de Recherche Expérimentale et Clinique, Université Catholique de Louvain, Brussels, Belgium[g]; Institute of Life Sciences Research and Technologies, Laboratoire Chimie et Biologie des Métaux, Grenoble, France[h]

The cell envelope of Gram-negative bacteria is an essential organelle that is important for cell shape and protection from toxic compounds. Proteins involved in envelope biogenesis are therefore attractive targets for the design of new antibacterial agents. In a search for new envelope assembly factors, we screened a collection of *Escherichia coli* deletion mutants for sensitivity to detergents and hydrophobic antibiotics, a phenotype indicative of defects in the cell envelope. Strains lacking *yciM* were among the most sensitive strains of the mutant collection. Further characterization of *yciM* mutants revealed that they display a thermosensitive growth defect on low-osmolarity medium and that they have a significantly altered cell morphology. At elevated temperatures, *yciM* mutants form bulges containing cytoplasmic material and subsequently lyse. We also discovered that *yciM* genetically interacts with *envC*, a gene encoding a regulator of the activity of peptidoglycan amidases. Altogether, these results indicate that YciM is required for envelope integrity. Biochemical characterization of the protein showed that YciM is anchored to the inner membrane via its N terminus, the rest of the protein being exposed to the cytoplasm. Two CXXC motifs are present at the C terminus of YciM and serve to coordinate a redox-sensitive iron center of the rubredoxin type. Both the N-terminal membrane anchor and the C-terminal iron center of YciM are important for function.

Antibiotic resistance has become a worldwide problem that threatens the effectiveness of many medicines used today to treat bacterial infections. A particularly serious threat is the emergence of Gram-negative pathogens, including *Escherichia coli* and *Pseudomonas aeruginosa*, which are resistant to all of the available antibacterial agents (1). It is therefore urgent to develop new antibiotics active against Gram-negative bacteria, which requires a deep understanding of the biology of these organisms. Proteins playing a role in the assembly of the cell envelope are attractive targets for antibiotic development because this structure is essential for viability and protection against toxic compounds such as antibiotics.

The envelope of Gram-negative bacteria is characterized by the presence of two concentric membranes, the inner membrane (IM) and outer membrane (OM), which are separated by the periplasm, a compartment that represents between 10 and 20% of the total cell volume and contains the peptidoglycan layer, or sacculus (2–4). The peptidoglycan sacculus is a heteropolymeric macromolecule composed of relatively short glycan strands and peptide cross-links, which serve to maintain cell morphology and give protection from turgor pressure. Although several proteins that play a key role in the biogenesis of the cell envelope have been identified recently (5–7), we have a poor understanding of how this complex architecture is assembled and of how envelope biogenesis is coordinated with cell growth and division. For instance, we do not know how the phospholipids that are present in the inner leaflet of the OM are transported across the periplasm and inserted in the membrane, and we have a partial understanding of the mechanisms that ensure the transport and insertion of β-barrel proteins in the OM (8).

A straightforward method to search for proteins involved in a particular process is to screen for mutants that exhibit defects that could result from an impairment of this process. As mutants with a decreased integrity of the envelope typically display an increased sensitivity to hydrophobic antibiotics and detergents (9), we screened a systematic collection of *E. coli* deletion mutants (the Keio collection) (10) for sensitivity to rifampin, a hydrophobic antibiotic, and to SDS. In this screen, we found that the mutant lacking *yciM*, a gene coding for a heat shock protein of unknown function (11), was one of the most sensitive strains of the Keio collection, suggesting severe defects in the cell envelope.

Further characterization of *yciM* mutants revealed that their growth is severely affected both by the osmolarity of the medium and by the temperature. Moreover, deletion of *yciM* leads to changes in cell morphology and to the formation of bulges that contain cytoplasmic material and cause cell lysis. We also uncovered a genetic interaction between *yciM* and *envC*, a gene coding for a protein involved in septation by controlling the activity of peptidoglycan amidases (12). Altogether, these results indicate that the presence of YciM is required for envelope integrity. The biochemical characterization of YciM revealed that the protein is

Received 14 August 2013 **Accepted** 25 October 2013
Published ahead of print 1 November 2013
Address correspondence to Jean-François Collet, jfcollet@uclouvain.be.
V.N. and H.E.H. are co-first authors of this article.
Supplemental material for this article may be found at http://dx.doi.org/10.1128/JB.00921-13.

doi:10.1128/JB.00921-13

anchored to the IM via a highly conserved N-terminal segment and that two C-terminal CXXC motifs serve to coordinate a redox-sensitive iron center of the rubredoxin type. Both the N-terminal transmembrane segment and the C-terminal iron center are important for YciM function.

MATERIALS AND METHODS

Bacterial strains and growth conditions. Bacterial strains are listed in Table S1. Strains CB23, VN26, NR1681, and VN250 were constructed by transferring the Δ*yciM*::*kan*, Δ*pyrF*::*kan*, Δ*yciS*::*kan*, and Δ*envC*::*kan* alleles, respectively, from the Keio collection (10) into the MC1000 wild-type strain using P1 transduction standard procedures (13). The kanamycin resistance cassette of strain CB23 was excised using pCP20 (14) to generate NR1647. Double mutants VN64, VN90, VN94, VN110, VN255, VN262, VN264, VN266, and VN268 were generated in the NR1647 strain by P1 transduction using alleles from the Keio collection. Strain VN15 is an *araD*$^+$ revertant of MC1000 selected on MacConkey agar supplemented with L-arabinose. The VN50 strain was constructed by transferring the Δ*yciM*::*kan* allele from the Keio collection into VN15 by P1 transduction. Unless otherwise noted, cultures were grown in LB medium (containing 1% NaCl) at 37°C. LB medium without NaCl (≤0.2%) was used for some experiments and is annotated as salt-free LB. When necessary, medium was supplemented with ampicillin (200 μg/ml), kanamycin (50 μg/ml), L-arabinose (0.2%), or D-glucose (0.2%). Growth was monitored by the optical density at 600 nm. We were unable to generate a Δ*yciM* Δ*envC*::*kan* double mutant by introducing into NR1647 the Δ*envC*::*kan* allele via P1 transduction and directly selecting for kanamycin-resistant transductants. However, we were able to construct the Δ*yciM* Δ*envC*::*kan* double mutant by cotransduction of the Δ*envC*::*kan* allele with a *zib563*::Tn*10* allele (~35% linkage) when we selected for tetracycline-resistant transductants.

Plasmid constructions. The plasmids and primers used in the present study are listed in Tables S1 and S2, respectively, in the supplemental material. Plasmid constructions are described in the supplemental material.

Sensitivity to antibiotics, detergents, bile salts, and osmotic stress conditions. To characterize the sensitivity of strains MC1000, CB23, and NR1681 to antibiotics, bacteria were grown in LB medium at 37°C. After 16 h, 100 μl of culture inoculum was mixed with 3 ml of molten LB top agar and poured over LB agar plates. BBL Sensi-Discs antimicrobial susceptibility test discs (6 mm) containing either rifampin (25 μg) or novobiocin (5 μg) were placed over the LB top agar, and the plates were incubated overnight at 37°C. The diameter of the zone of inhibition of growth around each disc was recorded in millimeters. The sensitivity to bile salts and osmotic stress was assayed by streaking isolated colonies of wild-type, *yciM*, *yciS*, and *pyrF* strains on MacConkey agar (which contains 0.15% bile salts) or on LB agar either lacking or containing 750 mM NaCl.

Complementation assays. VN15 and VN50 carrying plasmids pVN2 (YciM), pVN182 encoding a truncated YciM protein lacking the first 22 amino acids (YciM*), or pVN173 encoding YciM in which the four cysteines of the CXXC motif are replaced by serines (YciM$_{CCSSSS}$) were streaked on MacConkey agar or on salt-free LB agar and incubated at 22°C and 42°C, respectively.

Expression and purification. BL21(DE3) harboring the expression plasmid pHE72 encoding a C-terminally His-tagged version of YciM* (YciM$^*_{His}$), pVN55 encoding a C-terminally Strep-tagged version of YciM* (YciM$^*_{Strep}$), pVN74 (YciM*), pVN147 encoding a His-tagged mutant of YciM* in which the two cysteine residues outside the CXXC motif (Cys184 and Cys258) were replaced by serines (YciM$^*_{SS\text{/}CCCC-His}$), or pVN67 (YciM$^*_{SS\text{/}CCCC-Strep}$) was grown aerobically in LB medium at 37°C to an A_{600} of 0.5. Expression of the proteins was induced by adding 0.2% L-arabinose for YciM$^*_{His}$ and YciM$^*_{SS\text{/}CCCC-His}$ or 200 μg/liter of anhydrotetracycline for YciM$^*_{Strep}$, YciM*, and YciM$^*_{SS\text{/}CCCC-Strep}$. Shaking was resumed for 3 h. Cultures were then centrifuged for 20 min (8,000 × *g* at 4°C). From this point on, all steps were performed at 4°C. Bacteria expressing YciM$^*_{His}$ and YciM$^*_{SS\text{/}CCCC-His}$ were resuspended in 25 ml of buffer A (50 mM NaP_i, pH 8.0, 300 mM NaCl). Bacteria expressing YciM$^*_{Strep}$, YciM*, or YciM$^*_{SS\text{/}CCCC-Strep}$ were resuspended in 25 ml of buffer B (100 mM Tris, pH 8.0, 150 mM NaCl). Bacteria expressing YciM* were resuspended in 25 ml of buffer C (25 mM Tris, pH 8.0). Cells were then disrupted by two passages through a French press cell at 1,200 lb/in^2, and the cell lysate was centrifuged for 40 min (20,000 × *g* at 4°C). The resulting supernatant was then loaded on a 1-ml HisTrap HP column (GE Health Care) for YciM$^*_{His}$ and YciM$^*_{SS\text{/}CCCC-His}$, on a 5-ml Strep-Tactin column (IBA Tools) for YciM$^*_{Strep}$ and YciM$^*_{SS\text{/}CCCC-Strep}$, or on a Q-Sepharose column (GE Health Care) for YciM*. The columns were washed with buffer A, B, and C, respectively. YciM$^*_{His}$ and YciM$^*_{SS\text{/}CCCC-His}$ were eluted with a 0 mM to 300 mM imidazole gradient in buffer A, YciM$^*_{Strep}$ and YciM$^*_{SS\text{/}CCCC-Strep}$ were eluted with 2.5 mM desthiobiotin in buffer B, and YciM* was eluted with a 0 mM to 400 mM NaCl gradient in buffer C. The fractions containing the proteins were concentrated using a Vivaspin-15 device and desalted on a PD10 column (GE Health Care) equilibrated with buffer C. The fractions containing YciM$^*_{His}$, YciM$^*_{Strep}$, YciM$^*_{SS\text{/}CCCC-His}$, or YciM$^*_{SS\text{/}CCCC-Strep}$ were then loaded onto a Q-Sepharose column (GE Health Care) equilibrated with buffer C. The column was washed with buffer C, and the proteins were eluted with a 0 mM to 400 mM NaCl gradient in buffer C. The fractions containing the proteins were pooled and concentrated by ultrafiltration in an Amicon cell. The five different solutions containing each protein were then loaded on a Superdex 200 gel filtration column equilibrated with buffer D (25 mM HEPES, pH 7.1, 100 mM NaCl) at a flow rate of 0.5 ml/min. The fractions containing the proteins were concentrated, and the pure proteins were stored in buffer D. Optical spectra were recorded with a Varian Cary 50 Bio UV spectrophotometer.

Anaerobic purification. YciM$^*_{Strep}$ was expressed aerobically as described in the previous section. After centrifugation of the cultures for 20 min at 8,000 × *g* and 4°C, cells were broken anaerobically by two passages through a French press cell at 1,200 lb/in^2. The protein was then purified as explained above in an anaerobic tent containing 95% N_2 and 5% H_2. Optical spectra were recorded anaerobically with a Varian Cary 50 Bio UV spectrophotometer.

Subcellular localization of YciM. To determine the subcellular localization of YciM, BL21(DE3) cells harboring either the pVN2 (YciM), pVN182 (YciM*), or the pVN173 (YciM$_{CCSSSS}$) plasmid were grown in LB medium at 37°C to an A_{600} of 0.5. Expression of the proteins was induced by adding 0.2% L-arabinose. After 90 min, cultures were centrifuged for 20 min (8,000 × *g* at 4°C), and cell lysates were prepared as described above. The cell lysates were then ultracentrifuged 1 h at 100,000 × *g* at 4°C. The resulting supernatant containing the soluble proteins was stored. The pellet was resuspended in 15 ml of buffer A supplemented with 1% Triton X-100 and incubated at room temperature for 90 min. The solubilized proteins were then separated from the insoluble material by ultracentrifugation for 1 h at 100,000 × *g* at 4°C. The resulting supernatant containing the solubilized membrane proteins was kept for analysis.

Topology of YciM. To determine the orientation of the C-terminal part of YciM, BL21(DE3) cells harboring the pHE43 (YciM$_{His}$) expression plasmid were grown aerobically in LB medium at 37°C until an A_{600} of 0.4 was reached. Expression of the protein was induced by adding 0.2% L-arabinose. After 1 h, cells were centrifuged for 5 min at 8,000 × *g*, and the pellet was resuspended in 500 μl of 50 mM Tris buffer, pH 8.0. Spheroplasts were prepared by adding 1 volume of SP buffer (50 mM Tris, pH 8.0, 1 M sucrose, 2 mM EDTA, 0.5 mg/ml lysozyme). The mixture was then incubated at room temperature. After 15 min, $MgCl_2$ was added to a final concentration of 20 mM. Spheroplasts were collected by centrifugation at 13,000 × *g* for 10 min and resuspended in 500 μl of 50 mM Tris, pH 8.0, with or without Triton X-100 (0.2%). Proteinase K (50 μg/ml) was added to selected samples and incubated overnight at 37°C. Spheroplasts were then precipitated with 10% trichloroacetic acid (TCA) and left for 1 h on

ice. After a 10-min centrifugation at 16,000 × *g*, the precipitated material was washed with 5% TCA and finally resuspended in Laemmli buffer (15). Protein degradation was then analyzed by Western blotting using an anti-YciM antibody produced from a rabbit immunized with the purified protein (Eurogentec, Liège, Belgium).

Metal analysis. For the determination of the metal content of YciM, different preparations of YciM (50 μM each) were separated from exogenous metals by gel filtration using a PD10 column equilibrated with metal-free buffer (50 mM NaP_i, pH 8.0) prepared by incubation with Chelex 100 resin. The samples were concentrated 2-fold by ultrafiltration using a Centricon (Millipore) and analyzed using an inductively coupled plasma mass spectrometer (Agilent 7500cx), located at the Laboratory of Toxicology of the Université Catholique de Louvain in Brussels, Belgium. The metal content of the protein-containing retentate was compared with that of the filtrate. Zinc, nickel, iron, cobalt, arsenic, aluminum, selenium, cadmium, barium, lead, chrome, and manganese concentrations were measured. As additional controls, buffer samples were analyzed using the same procedure.

PAR-PMPS assay. Zinc concentration was determined using the zinc-complexing reagent PAR (4-(2-pyridylazo)resorcinol). PAR binds zinc to form a $Zn(PAR)_2$ complex, which absorbs strongly at 500 nm ($\varepsilon = 66{,}000\ M^{-1}\ cm^{-1}$ in HEPES, pH 7.0). To determine the amount of zinc bound to the protein, *p*-hydroxymercuriphenylsulfonic acid (PMPS) was added to release zinc from the zinc center and allow the formation of the $Zn(PAR)_2$ complex. PMPS forms mercaptide bonds with thiols using the following reaction mechanism: R-HgOH + P-SH → R-Hg-S-P + H_2O, where the R stands for the phenylsulfonic acid group of PMPS and the P stands for a protein. This reaction mechanism proceeds as a substitution reaction whereby the hydroxyl anion is displaced by the thiol-containing protein to form a mercuric sulfide derivative of the protein (R-Hg-S-P). If the thiols on the protein are involved in coordinating a metal such as zinc, this covalent modification leads to the release of the zinc. To determine the number of cysteines involved in zinc binding, defined amounts of PMPS are added, and the changes in A_{500} are recorded (16, 17).

Sulfur content analysis. The sulfur content of $YciM^{*}_{Strep}$ was determined using a colorimetric assay described by Beinert et al. (18). Standard curves were established using a sodium sulfur solution (Na_2S).

Microscopy. For cell length analysis using phase-contrast microscopy, wild-type and *yciM* strains were grown at 37°C to exponential phase, placed on a 2% LB agarose pad, and mounted on a Nikon Ti-Eclipse inverted microscope equipped with a TI-CT-E motorized condenser and a CoolSnap HQ2 FireWire charge-coupled-device (CCD) camera. The cell length analysis was performed using the free, open-source software MicrobeTracker (19). This software package was specifically designed to detect and outline bacterial cells in microscopy images. To perform time-lapse microscopy, wild-type and *yciM* cells were grown at 37°C to an A_{600} of 0.5 and placed on a microscope slide layered with a pad of 1% agarose containing LB medium with different salt concentrations. These slides were placed on a microscope stage at different temperatures. Samples were observed using differential interference contrast (DIC) or phase-contrast imaging on a Nikon Eclipse E1000 microscope with a 100× objective and monitored with a Hamamatsu ORCA-ER LCD camera. Images were taken every 3 min and then processed with NIS Elements AR, version 3.0, software (Nikon). To generate images for Fig. S1 in the supplemental material, strains were grown on LB plates at 37°C overnight. Colonies were resuspended in LB medium, and cells were layered on an 1% agarose pad containing phosphate-buffered saline (PBS), pH 7.4 (137 mM NaCl, 2.7 mM KCl, 8 mM Na_2HPO_4, 1.46 mM KH_2PO_4), and imaged using phase-contrast with a 100× oil immersion objective lens and a Nikon Eclipse Ti-E microscope equipped with a Nikon DS-QI1 cooled digital camera.

Fluorescence microscopy. To determine whether the bulges contain cytoplasmic material, HE89 cells were grown in LB medium at 37°C until an A_{600} of 0.5 was reached. Then, time-lapse microscopy was performed by placing the strains on a microscope slide that was layered with a pad of 1% agarose-containing LB medium. After the temperature was shifted to 42°C, DIC and fluorescence images were taken every 3 min. Fluorescence was observed with a BrightLine fluorescein isothiocyanate (FITC) filter set. To determine the localization of YciM and YciM* with a C-terminal fusion of the fluorescent protein mCherry ($YciM_{mCherry}$ and $YciM^{*}_{mCherry}$, respectively), HE64 and VN237 cells were grown in LB medium at 37°C to an A_{600} of 0.5. Production of $YciM_{mCherry}$ or $YciM^{*}_{mCherry}$ was induced by adding L-arabinose to a final concentration of 0.2%. After 30 min, the bacteria were placed on a microscope slide layered with a pad of 1% agarose. Fluorescence was observed with a BrightLine TXRED-4040B filter set.

RESULTS

Deletion of *yciM* severely impairs the integrity of the cell envelope. To identify new proteins involved in maintaining the integrity of the cell envelope, we screened the Keio collection for sensitivity to detergents and hydrophobic antibiotics, a phenotype indicative of envelope defects (9). The Keio collection is a systematic collection of *E. coli* deletion mutants that contain disruptions in 3,985 nonessential genes, including several hundreds of uncharacterized open reading frames (10). We streaked the mutants on LB plates containing either rifampin, a hydrophobic antibiotic which does not cross the OM easily (9), or a mixture of SDS and EDTA. EDTA complexes the cations inserted between the lipopolysaccharide (LPS) molecules and therefore destabilizes the OM, rendering the bacteria more sensitive to the detergent. Only 42 strains were sensitive to both SDS-EDTA and rifampin (see Table S3 in the supplemental material). Most of the sensitive mutants corresponded to genes already known to be involved in envelope assembly, such as mutants defective in LPS biosynthesis (*rfaC*, *rfaD*, *rfaE*, *rfaF*, *rfaH*, *rfaI*, and *rfaP* mutants) or in β-barrel insertion at the OM (*surA*, *bamB*, and *bamE* mutants), which validated our experimental approach (20, 21). Four mutants lacked proteins of unknown function (*yciM*, *yfgC*, *yraP*, and *ybiX* mutants) although recently YfgC has been implicated in the degradation of misfolded β-barrel proteins at the OM (22). We tested the sensitivity of these four mutants to other hydrophobic antibiotics and found that strains lacking *yciM* were the most sensitive (see Table S4), which prompted us to investigate the properties of the *yciM* mutant and to characterize the corresponding protein.

Characterization of the *yciM* mutant. For our studies, we introduced the Δ*yciM*::*kan* allele from the Keio collection into MC4100 and MC1000, two well-characterized *E. coli* strains (23, 24). When we transferred the Δ*yciM*::*kan* allele in strain MC4100, we observed that the resulting mutant exhibited growth defects and accumulated suppressors rapidly. This strain was therefore not retained for further studies. In contrast, the Δ*yciM*::*kan* allele could be stably transduced into MC1000 (23). As shown in Table 1, and similar to the *yciM* strain from the Keio collection, the MC1000 *yciM* mutant exhibits increased sensitivity to rifampin and novobiocin, two hydrophobic antibiotics (Table 1), and to a mixture of SDS and EDTA.

We then investigated the growth properties of the MC1000 *yciM* mutant under various temperature and culture conditions and found that deletion of *yciM* causes a pleiotropic phenotype in *E. coli*. First, *yciM* mutants are unable to grow at low temperatures on MacConkey agar, a medium containing bile salts (Fig. 1A). Second, *yciM* mutants are sensitive to high salt concentrations, being unable to grow on LB medium containing 750 mM NaCl at 37°C (Table 1). Third, *yciM* mutants display a thermosensitive growth defect in low-osmolarity medium, being unable to grow at

TABLE 1 Sensitivity of the MC1000 *yciM* and *yciS* mutants to antibiotics, SDS-EDTA, and osmotic stress conditions

Strain	Inhibition zone (mm) with:		Growth on LB plates with:[a]	
	Rifampin (25 μg)	Novobiocin (5 μg)	0.05% SDS–1.25 mM EDTA	750 mM NaCl
Wild type	12 ± 0.5	< 6	+++	+++
yciM strain	16 ± 1.2	19 ± 3.1	−	−
yciS strain	13 ± 1.2	7.6 ± 1.5	+	+++

[a] Strains were streaked on plates containing the additives shown. Growth is reported from normal growth (+++) to no growth (−) after overnight incubation at 37°C.

42°C in low-salt LB liquid culture (Fig. 1B) and on salt-free LB agar (Fig. 1C). These mutants also exhibit a heat-sensitive phenotype at 45°C in LB liquid cultures (data not shown). These phenotypes are not caused by polar effects since mutants lacking *pyrF*, the gene located immediately downstream of *yciM* on the chromosome, are not sensitive to antibiotics, are able to grow on MacConkey plate at 22°C (Fig. 1A), and do not exhibit a thermosensitive growth defect on salt-free LB agar (Fig. 1C). Furthermore, expressing the wild-type YciM protein from a plasmid rescues the inability of the *yciM* mutant to grow on MacConkey agar at 22°C (Fig. 1A) and on salt-free LB agar at 42°C (Table 2). Thus, the aforementioned phenotypes are the result of the loss of YciM.

As *yciM* has been reported to form a heat-inducible operon with *yciS* (11, 25), a gene encoding a small-membrane protein of unknown function (26), we investigated the phenotypes of the *yciS* mutant. Note that *yciS* is located upstream of *yciM* on the chromosome. Although *yciS* mutants are moderately sensitive to antibiotics and detergents (Table 1), their growth is not affected by modulating the salt concentration of the medium (Table 1) or the temperature (data not shown), indicating that YciS is not required for the full function of YciM. Thus, *yciS* was not considered further in the present study.

***yciM* mutants have an increased cell length and form bulges at elevated temperatures.** We then explored the morphology of the *yciM* mutants microscopically. First, we observed that there is a significant heterogeneity in the cell length of *yciM* mutants compared to the wild type (Fig. 2A) and that the average length of *yciM* mutant cells is ~1.7-fold increased ($n = 300$) compared to the length of wild-type cells (from 4.45 ± 0.84 to 7.57 ± 3.98 μm; $n = 300$). The increase in length does not seem to result from failures in the division process as *yciM* mutant cells divide normally (see Movie S1 in the supplemental material). Moreover, using time-lapse microscopy, we observed that bacteria lacking *yciM* form bulges that are mostly localized at the division site and whose formation leads to cell lysis. Whereas only a small number of the cells (~3%) were found to form bulges at 37°C, the number of bulging cells increases about 3-fold at 42°C (Fig. 2B). To check if the bulges contain cytoplasmic materials, green fluorescent protein (GFP) was constitutively expressed in the cytoplasm. The fluorescent protein was clearly visible within the bulges and then scattered in the environment upon lysis (Fig. 2D). This result strongly suggests that bulge formation involves both the IM and the OM and indicates that the bulges contain cytoplasmic materials.

We also explored the effects of various salt concentrations on the growth and morphology of the *yciM* mutant at the single-cell level. On salt-free LB agar at 42°C (Fig. 2C), we observed that *yciM*

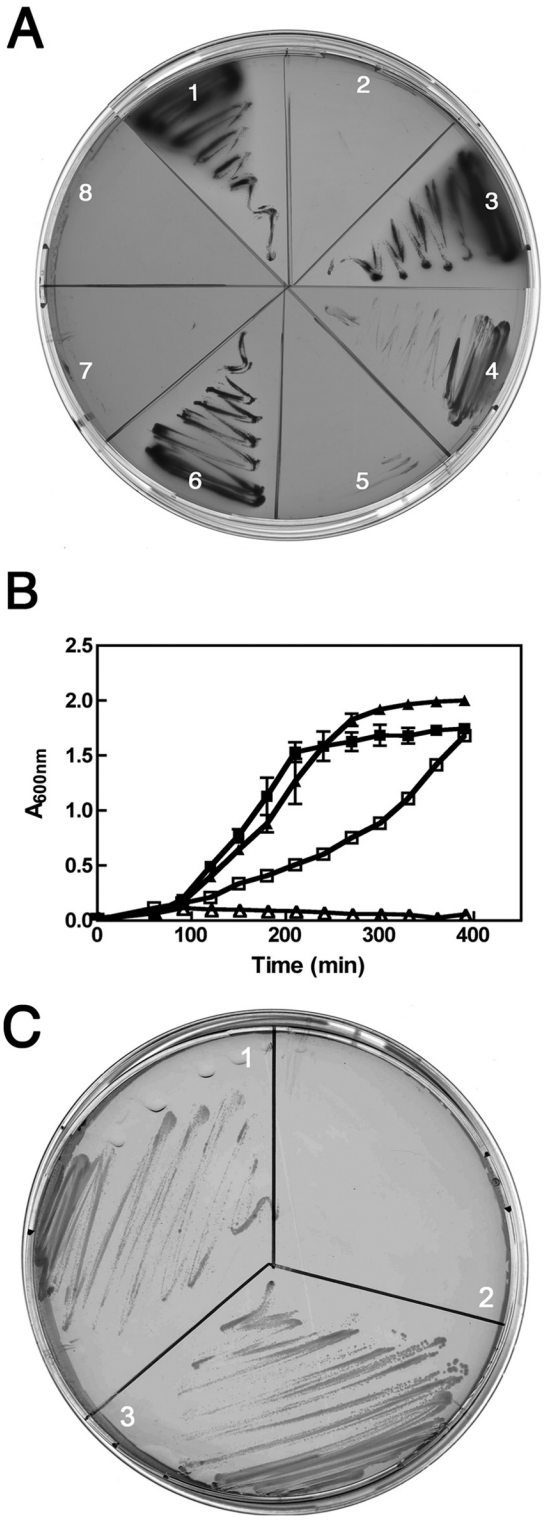

FIG 1 Characterization of the *yciM* mutant. (A) The growth of wild-type (1), *yciM* (2), and *pyrF* strains (3) on MacConkey agar was evaluated at 22°C. The ability of the various YciM constructs to complement the growth defect of *yciM* mutants on MacConkey agar at 22°C was tested by expressing YciM (4), YciM* (7), or $YciM_{CCSSSS}$ (8). Wild-type (6) and *yciM* mutant (5) strains harboring the control pBAD-HisB plasmid were also analyzed. (B) Growth curves of wild-type (■) and *yciM* (▲) strains at 42°C in LB medium (filled symbols) or in salt-free LB medium (open symbols). (C) The growth of wild-type (1), *yciM* (2), and *pyrF* (3) strains was evaluated at 42°C on salt-free LB plates.

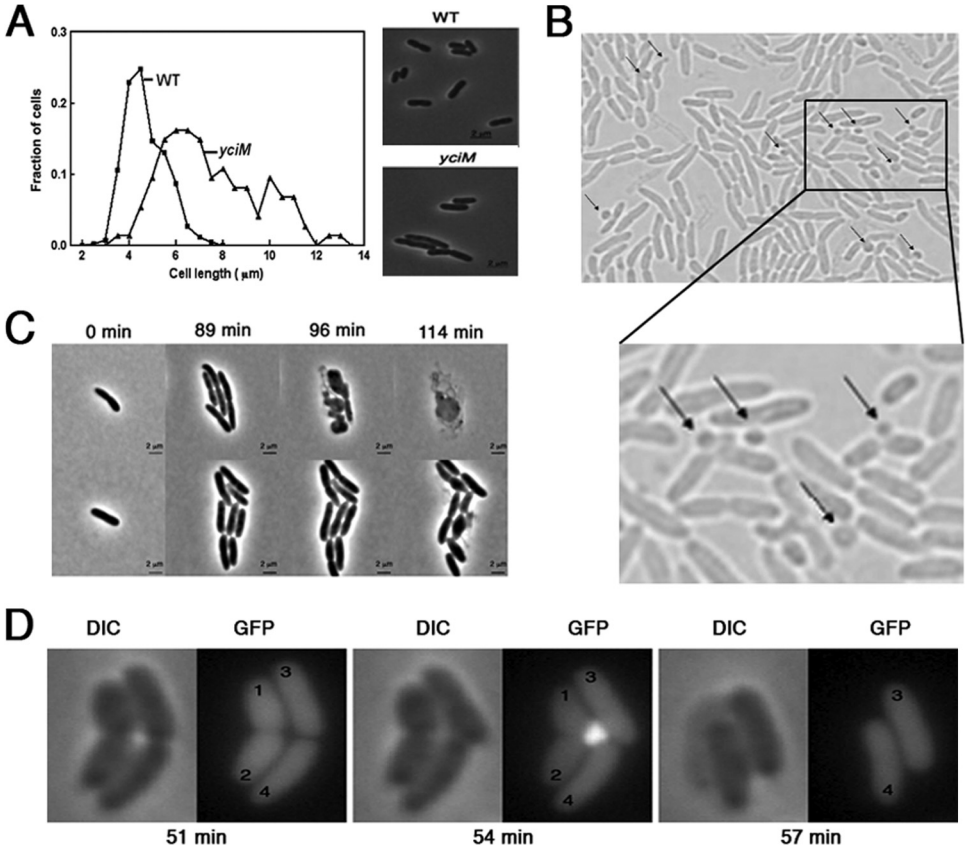

FIG 2 Loss of YciM causes morphological defects. (A) Wild-type and *yciM* strains grown at 37°C to exponential phase were placed on a 2% LB agarose pad. Phase-contrast images of 300 random cells were recorded, and the MicrobeTracker open-source software (19) was used to determine the length of individual cells. (B) *yciM* mutants were placed on a microscopy slide layered with a 1% agar pad containing LB medium. Bacteria were grown for 3 h at 42°C, and pictures were taken every 3 min using DIC. Bulges appear after about 60 min and are indicated by the black arrows. A enlarged image is shown in the lower part of the panel. (C) Phase-contrast images of wild-type (lower row) and *yciM* strains (upper row) grown on salt-free LB-agar medium at 42°C. *yciM* mutant cells have an altered morphology and lyse after a few divisions, whereas growth of the wild-type strain is only slightly affected. (D) DIC and fluorescence image (GFP) of strain HE89 (*yciM* mutant constitutively expressing cytoplasmic GFP from pFPV25) grown at 42°C. The displayed sequential images were taken 51 min after the shift from 37°C to 42°C. The presence of GFP in the bulges indicates that they involve both the IM and the OM and contain cytoplasmic materials. The cells numbered 1 and 2 lyse following bulge formation.

mutant cells have irregular shapes and lyse after a few cell divisions (Fig. 2C). When grown on LB with high salt concentrations at 37°C, cells lacking *yciM* also rapidly lyse, sometimes following bulge formation (not shown).

***yciM envC* null alleles exhibit a synthetic phenotype.** The phenotypes of the *yciM* mutant described above are consistent with defects in the envelope, suggesting that loss of YciM alters envelope integrity. To obtain more information on the envelope assembly process specifically impacted by *yciM* deletion, we investigated whether *yciM* exhibits genetic synthetic interactions with null alleles of genes involved in envelope biogenesis. We focused on genes involved in LPS biosynthesis (*rfaQ*, *rfaP*, *asmA*, and *rfaI*) and peptidoglycan assembly (*prc*, *envC*, *mrcA*, *ponB*, *pbpC*, and *nlpD*) because the increased sensitivity to antibiotics and lysis reported above could result from defects in either pathway. Out of the 10 alleles tested, we found that only the inactivation of *envC* in the *yciM* mutant results in a synthetic phenotype. Initially, we were unable to introduce the Δ*envC*::*kan* allele using P1 transduction by directly selecting for kanamycin resistance, suggesting that these alleles might be a synthetic lethal pair. However, we could generate the Δ*yciM* Δ*envC*::*kan* double mutant by cotransducing at the expected ~35% frequency the Δ*envC*::*kan* allele with a nearby *zib563*::Tn*10* allele when we selected for tetracycline-resistant transductants. This indicates that *yciM* and *envC* are not synthetic lethal. However, as shown in Fig. S1 in the supplemental material, *yciM envC* mutant cells exhibit aberrant morphology and often lyse, suggesting that they have severe cell envelope defects.

TABLE 2 Complementation assays on salt-free LB medium

Strain	Growth on salt-free LB plates at 42°C[a]
Wild type (pBAD-HisB)	+++
yciM (pBAD-HisB) strain	−
yciM (pBAD-HisB-YciM) strain	+++
yciM (pBAD-HisB-YciM*) strain	−
yciM (pBAD-HisB-YciM$_{CC/SSSS}$) strain	−

[a] The ability of the various YciM constructs to complement the growth defect of *yciM* mutants on salt-free LB medium at 42°C was tested. Wild-type and *yciM* mutant strains harboring the control pBAD-HisB plasmid were also analyzed. +++, normal growth; −, no growth.

As the function of EnvC is to activate AmiA and AmiB (12), two peptidoglycan amidases that cooperate in septal peptidoglycan splitting, we tested whether *yciM* also genetically interacts with the genes coding for these two hydrolytic enzymes. We could construct the *yciM amiA* and *yciM amiB* double mutants. However, we were unable to construct the *yciM amiA amiB* triple mutant by selecting for kanamycin-resistant Δ*amiA*::*kan* transductants using a *yciM amiB* strain as recipient. Because *yciM* and *envC* are not synthetic lethal, the inability to construct this *yciM amiA amiB* triple mutant strain is likely caused by the same unknown reason for which we cannot select for kanamycin-resistant Δ*envC*::*kan* transductants in a *yciM* mutant. Together, these phenotypes suggest that YciM is connected to peptidoglycan homeostasis (see Discussion).

YciM localizes to the IM. YciM is a 44.5-kDa protein (Fig. 3A) which is annotated in the databases as a protein secreted to the periplasm. YciM presents, indeed, a highly hydrophobic N-terminal domain predicted to be a signal sequence by several computational methods such as Psort and SignalP (27). However, most periplasmic targeting sequences consist of a short, positively charged amino-terminal segment, followed by a longer hydrophobic domain (28). It is the hydrophobic character of this domain that is usually conserved, rather than the amino acid sequence. The sequence of the N-terminal domain of YciM does not fit well with that description: no positively charged residue is present among the first 20 amino acids. Moreover, although the sequence of the predicted export signal is hydrophobic, it is highly conserved among YciM homologues (Fig. 3B). These observations suggest that, instead of corresponding to a signal sequence that is released from the protein after export, the N-terminal segment of YciM could serve as a transmembrane α-helix anchoring the protein in the IM. We expressed both the full-length protein and a truncated version lacking the first 22 amino acids (YciM*) and studied their subcellular localizations. The wild-type protein was present in the membrane fraction, whereas YciM* was found in the soluble fraction (Fig. 4A). In a parallel approach, we fused the C terminus of YciM to the fluorescent protein mCherry. As shown in Fig. 4B, YciM$_{mCherry}$ localizes in the membrane while YciM$^*_{mCherry}$ localizes in the cytoplasm. Thus, YciM is a membrane protein that is anchored in the IM by its N-terminal sequence. Interestingly, expression of YciM* is unable to rescue growth of the *yciM* mutant on MacConkey agar at 22°C (Fig. 1A), indicating that the N-terminal domain that anchors YciM to the membrane is required for its activity.

The presence of two arginine residues (Arg21 and Arg22) located immediately after the transmembrane α-helix suggests that the protein is oriented toward the cytoplasm (28). To confirm this topological orientation of YciM, spheroplasts were prepared from cells expressing YciM and incubated with proteinase K. As shown in Fig. 4C, YciM becomes accessible to the protease only when the membrane is solubilized with Triton X-100, thus confirming the cytoplasmic orientation of the protein.

YciM is a metal-binding protein. There are two CXXC motifs at the C terminus of YciM (Fig. 3B). BLAST searches using the carboxy-terminal part of YciM revealed that this region is conserved in all YciM homologues (Fig. 3B) and aligns with the zinc-binding cysteine residues of the DNA repair protein RadA (not shown) (29). To test whether the CXXC motifs of YciM are also involved in zinc binding, we prepared a C-terminally His-tagged version of YciM* (YciM$^*_{His}$) to purify the protein by affinity chromatography. The fractions containing YciM$^*_{His}$ were then successively loaded on a Q-Sepharose anion-exchange chromatography column and a Superdex S200 gel filtration column. After these steps, the protein was pure to near homogeneity (one minor contaminant, identified as the chaperone DnaK, was also present in the YciM-containing fractions) (see Fig. S2 in the supplemental material). The purified protein was then used to study the metal content of YciM. YciM$^*_{His}$ was separated from free metals by gel filtration against metal-free buffer, and the metal content was analyzed by inductively coupled plasma-high-resolution mass spectrometry (ICP-HRMS). We found that zinc is present in the protein in a 1:1 molar stoichiometry (1.1 zinc/protein). No other metals were detected in the protein preparation.

Cysteines and histidines are frequently involved in zinc coordination. YciM contains six cysteine residues, including four in the carboxy-terminal region, and eight histidine residues. To determine if and how many cysteine residues are involved in zinc binding, we used the PAR/PMPS assay (16, 17). PAR is a dye that chelates zinc to form a red Zn(PAR)$_2$ complex. This complex absorbs at 500 nm, and its formation can therefore be easily monitored. However, because the affinity of PAR for zinc (affinity constant [K_a], 2×10^{12} M^{-1}) is lower than the affinity of most protein zinc centers (usually $>10^{14}$ M^{-1}), tightly bound zinc cannot be extracted by PAR, and thiol-modifying reagents such as PMPS are used.

When freshly purified YciM was incubated with PAR, we did not observe a significant increase in the A_{500}, indicating that PAR was unable to extract the zinc from the protein. Stepwise additions of PMPS led to a progressive increase in the A_{500} (see Fig. S3 in the supplemental material), and zinc was fully released when four cysteine residues were titrated. This indicates that zinc is coordinated to YciM via four cysteine residues.

To determine whether the zinc-binding cysteine residues correspond to the four cysteines of the CXXC motifs, we purified a mutant version of YciM* in which the two cysteine residues outside the CXXC motifs (Cys184 and Cys258) were replaced by serines (YciM$^*_{SS/CCCC-His}$). ICP-HRMS analysis showed that YciM$^*_{SS/CCCC-His}$ contains zinc in a 1:1 ratio, indicating that zinc is bound to YciM via the cysteines of the two CXXC motifs. This is consistent with the fact that Cys184 and Cys258 are not highly conserved (Fig. 3B), in contrast to the cysteine residues of the CXXC motifs.

YciM contains an iron cluster. In the course of the project, we serendipitously purified YciM on a Strep-Tactin column by taking advantage of a Strep tag fused at the C terminus of the protein instead of a His tag. Surprisingly, the protein that eluted from the Strep-Tactin column, which was pure to near homogeneity, appeared bright pink, suggesting that it might bind iron (see Fig. S4 in the supplemental material). Whereas no peaks were observed in the visible range for YciM$^*_{His}$, the absorbance spectrum of purified YciM$^*_{Strep}$ (Fig. 5A) shows a large peak around 500 nm and a smaller, narrow peak around 410 nm. We determined the metal content of YciM$^*_{Strep}$ and found that both iron and zinc were present in 0.11 and 0.44 molar ratios, respectively. We tested whether Cys184 and Cys258 are involved in iron binding by expressing YciM$^*_{SS/CCCC}$ fused to a Strep tag (YciM$^*_{SS/CCCC-Strep}$). However, replacement of Cys184 and Cys258 by serine residues does not alter

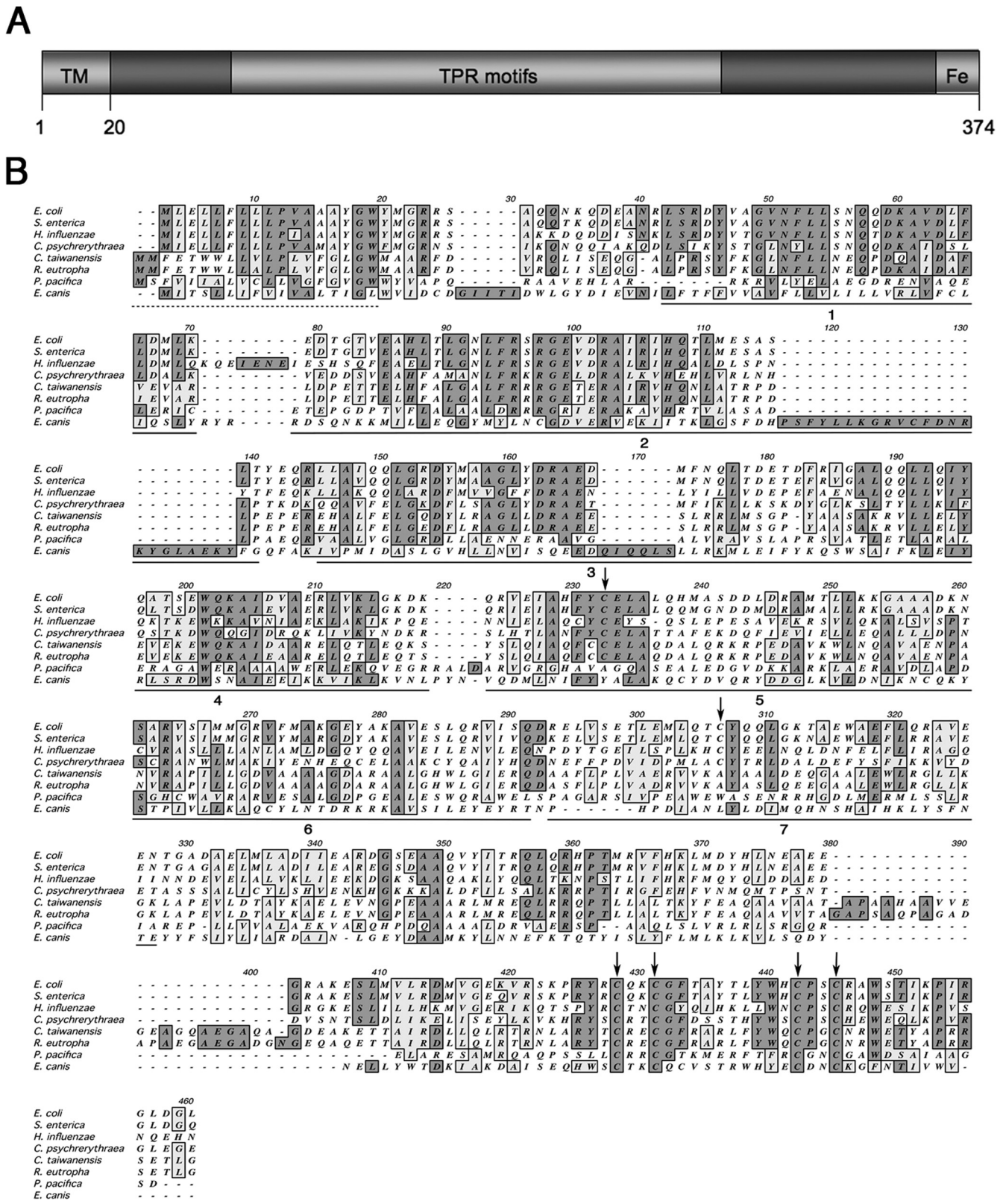

FIG 3 Structural features of the YciM sequence. (A) YciM is a multidomain protein: the N-terminal part (transmembrane, TM) anchors the protein in the IM, the central part of the protein presents several TPR motifs that most likely mediate protein-protein interactions, and the C terminus presents two CXXC motifs that bind iron (Fe). (B) Multiple sequence alignment of *E. coli* YciM with homologous proteins from other Gram-negative bacteria from the *Alpha-*, *Beta-*, *Gamma-*, and *Deltaproteobacteria*. The N-terminal domain (underlined with the dashed line) is hydrophobic and highly conserved. All YciM proteins contain seven TPR motifs (marked from 1 to 7). The conserved iron-binding CXXC motifs are present at the C terminus (cysteine residues are marked with arrows). The sequences of *Escherichia coli* (UniProtKB accession no. P0AB58), *Salmonella enterica* (B5PPH9), *Haemophilus influenzae* (Q4QJV0), *Colwellia psychrerythraea* (Q482G0), *Ralstonia eutropha* (Q0KDH3), *Cupriavidus taiwanensis* (B3R3B7), *Plesiocystis pacifica* (A6G5X1), and *Ehrlichia canis* (Q3YT24) were aligned using Clustal W2.

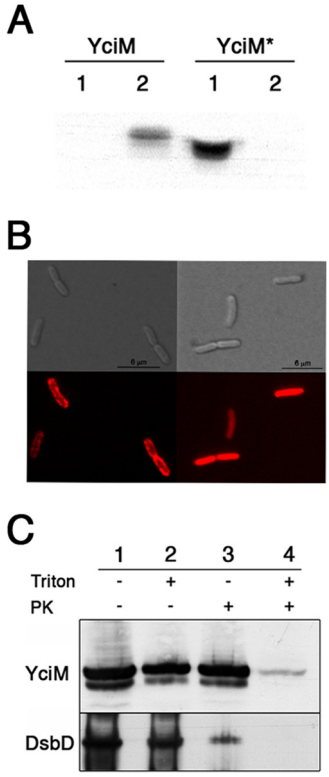

FIG 4 YciM is an inner membrane protein. (A)*E. coli* cells expressing YciM (VN241) or YciM* (VN198) were fractionated. YciM and YciM* were detected using an anti-YciM antibody (lane 1, soluble fraction; lane 2, membrane fraction). (B) DIC images (upper panel) and the corresponding fluorescence images (lower panel) of HE64 (expressing $YciM_{mCherry}$) and VN237 (expressing $YciM^{*}_{mCherry}$) strains. $YciM_{mCherry}$ localizes in the membrane (left panel), whereas $YciM^{*}_{mCherry}$ is present in the cytoplasm (right panel). Images were taken 30 min after the induction of the fluorescent proteins by addition of 0.2% L-arabinose. (C) Spheroplasts prepared from bacteria expressing YciM (VN241) were solubilized or not with Triton X-100 (1%) and then incubated with proteinase K (PK) as indicated. YciM was detected by Western blotting using an anti-YciM antibody. The fact that YciM is not degraded by proteinase K in the absence of Triton X-100 indicates that YciM is oriented toward the cytoplasm. DsbD, an inner membrane protein, was used as a control. DsbD was detected using an anti-DsbD antibody.

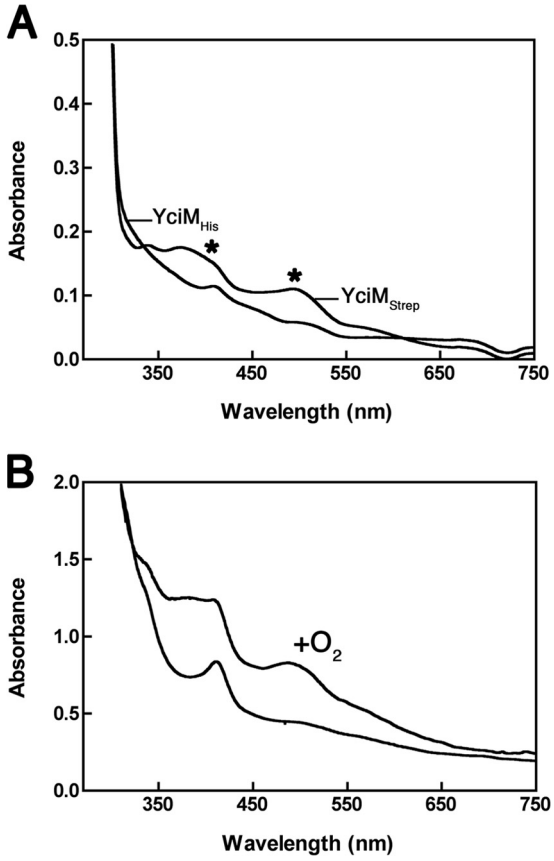

FIG 5 YciM is a metal binding protein. (A) UV-visible light absorption spectra of purified $YciM^{*}_{Strep}$ and $YciM^{*}_{His}$ (150 μM). The absorbance was measured between 250 nm and 750 nm. The spectrum of $YciM^{*}_{Strep}$ shows a large peak around 500 nm and a smaller one around 410 nm (marked with asterisks). (B) $YciM^{*}_{Strep}$ was purified on a Strep-Tactin column under anaerobic conditions. The protein that eluted from the column was yellow, and its absorbance spectrum presented a peak at 410 nm (lower curve). Exposure of the protein to oxygen turned it pink, presenting an absorbance peak around 500 nm (upper curve, + O_2). The protein concentration was about 250 μM.

the pink appearance of the protein and has no impact on the metal content, indicating that iron is also bound to YciM via the two C-terminal CXXC motifs. We confirmed the results obtained on $YciM^{*}_{Strep}$ by purifying a nontagged version of the protein ($YciM^{*}$). After purification of $YciM^{*}$ to homogeneity using ion exchange and size exclusion chromatography, the protein was found to contain iron and zinc in a ratio similar to that of $YciM^{*}_{Strep}$. Thus, the CXXC motifs of YciM are able to bind iron and/or zinc. In the Discussion, we explain why we think that iron, not zinc, is the metal which is coordinated by YciM *in vivo*. From now on, we will refer to YciM as an iron-binding protein. Because iron-binding centers are usually sensitive to oxygen, we also purified $YciM^{*}_{Strep}$ anaerobically to see whether purification of the protein in the absence of oxygen would increase the iron-to-zinc ratio, which was not observed. Interestingly, while YciM is a slightly yellow protein under anaerobic conditions, exposure to oxygen turns it into a pink protein displaying the typical absorbance peak around 500 nm (Fig. 5B). This indicates that the iron center of YciM is redox sensitive.

YciM has an iron center of the rubredoxin type which is required for protein stability. CXXC motifs have been shown to be involved both in the coordination of iron-sulfur clusters and in the coordination of iron centers of the rubredoxin type (30). Analysis of the sulfur content of YciM by a colorimetric assay revealed that YciM does not contain any inorganic sulfur (data not shown), indicating that YciM binds an iron center of the rubredoxin type. This is further supported by the fact that the absorbance spectrum of $YciM^{*}_{Strep}$ resembles that of other rubredoxin proteins (31, 32). We produced a mutant version of YciM in which the four cysteines of the CXXC motifs are replaced by serines ($YciM_{CCSSSS}$). This mutant mostly accumulates in inclusion bodies (data not shown), indicating that the metal center is required for the stability of the protein. However, as a significant portion of $YciM_{CCSSSS}$ still localizes to the membrane, we tested whether it can rescue the growth defect of the *yciM* mutant on either MacConkey agar at 22°C or salt-free LB at 42°C. As shown in Fig. 1A and Table 2, we observed that the fraction of $YciM_{CCSSSS}$ present in the membrane is unable to complement the *yciM* mutant, suggesting that the redox-sensitive iron center of YciM is important for YciM function.

DISCUSSION

In this study, we have demonstrated that YciM, a protein required for maintenance of cell envelope integrity in *E. coli*, contains two domains essential for function: an N-terminal transmembrane domain that anchors YciM to the IM and a C-terminal cytoplasmic domain that contains seven tetratricopeptide repeat (TPR) motifs and an iron cluster required for function. We have also described phenotypes associated with the loss of YciM that reveal both OM and peptidoglycan defects. Furthermore, its cellular localization and structural features suggest that YciM is likely to function in envelope biogenesis in association with other proteins that are yet to be identified.

YciM is anchored to the IM by a hydrophobic N-terminal domain that contains residues highly conserved among bacterial species from the *Alpha-*, *Beta-*, *Gamma-*, and *Deltaproteobacteria* (Fig. 3B). This high degree of conservation and the fact that this domain is required for YciM function suggest that it might mediate interactions between YciM and other polypeptides present in the IM. YciM also contains seven TPR motifs localized to the cytoplasm (Fig. 3B). TPR motifs serve in a variety of protein-protein interactions (33), which further suggests that YciM is involved in a multiprotein complex. Future studies targeting the identification of putative interacting partners may reveal the function that YciM plays in envelope biogenesis.

Another structural feature of the C-terminal portion of YciM is a metal center coordinated by four cysteine residues. Although we first identified zinc as the metal coordinated by the two CXXC motifs present in YciM, the protein also binds iron when the His tag is removed. Our results suggest that the His tag, which is located immediately downstream of the metal-chelating cysteines, interferes with the stability of the iron center in YciM, leading to the replacement of iron by zinc. The low iron content of $YciM^{*}_{Strep}$ and $YciM^{*}$ very likely results from the notoriously low stability of iron centers, which often leads to the replacement of iron by zinc during protein overexpression and purification (34–36). Importantly, we have demonstrated that this iron center is essential for YciM function although whether it plays a structural or redox-related role remains unknown.

The sensitivity of *yciM* mutants to hydrophobic antibiotics and detergents results from an increased permeability of the OM, suggesting a defect in OM biogenesis (9). However, we have also uncovered phenotypes indicating that *yciM* mutants have defects in peptidoglycan biogenesis. First, the fact that *yciM* mutants have irregular shapes and lyse following bulge formation supports the presence of defects in the peptidoglycan layer (37). It has indeed been shown that bulge formation results from a defective peptidoglycan assembly leading to the formation of a weakened area in the peptidoglycan layer. For instance, treatment of *E. coli* with antibiotics that inhibit peptidoglycan synthesis, such as β-lactams, as well as overexpression of inactive variants of enzymes involved in peptidoglycan assembly causes bulge-induced lysis (38–40). Second, the sensitivity of the *yciM* deletion mutants to low-osmolarity medium is also consistent with defects in the peptidoglycan as a similar phenotype has been reported for mutants impaired in peptidoglycan assembly and/or cell division (41, 42). For instance, cells lacking FtsEX, an IM complex that recruits EnvC to the septum, also display a division defect in LB medium of low osmotic strength (43). Third, the facts that the simultaneous deletion of *yciM* and *envC*, a gene coding for a regulator of peptidoglycan hydrolysis (44, 45), leads to severe morphological defects and that *yciM* mutants are more sensitive to β-lactams (46) also support a role for YciM in peptidoglycan assembly. Nevertheless, although these phenotypes indicate that the loss of YciM leads to defects in peptidoglycan, we have also observed the aforementioned permeability phenotypes that are consistent with OM defects. In Gram-negative bacteria, the OM and peptidoglycan layer are intimately associated. For example, the Lpp OM lipoprotein covalently anchors the OM to the peptidoglycan layer (47, 48), while the OM lipoproteins LpoA and LpoB are needed for the proper synthesis of the peptidoglycan layer (49, 50). Consequently, defects in the biogenesis of one can affect the biogenesis of the other. Because the present studies cannot discriminate which of the reported defects are the primary consequence of the loss of YciM, additional work is required to understand the role that YciM plays in envelope biogenesis.

ACKNOWLEDGMENTS

We thank Asma Boujtat and Geneviève Connerotte for their excellent technical assistance, William Cenens (Katholieke Universiteit Leuven, Leuven, Belgium), Michael Deghelt (University of Namur, Namur, Belgium), and Emily K. Butler (The Ohio State University, USA) for the microscopy experiments, and Sander Govers (Katholieke Universiteit Leuven, Leuven, Belgium) for the cell length analysis. We also thank P. Rolf Thauer and Seigo Shima (Max-Planck Institute for Terrestrial Microbiology, Marburg, Germany) for their help in the anaerobic purification of YciM as well as Tricia Kiley, Benjamin Ezraty, and Frederic Barras for insightful discussions regarding YciM.

J.F.C. is Maître de Recherche of the FRS-FNRS. V.N. and M.D. are research fellows of the FRIA. P.L. is Chargée de Recherche of the FRS-FNRS. This work was supported by grants from the FRS-FNRS to J.-F.C. and the National Institute of General Medical Sciences of the National Institutes of Health under award number R01GM100951 (to N.R.), and start-up funds from The Ohio State University (to N.R.).

REFERENCES

1. **Gould IM.** 2008. The epidemiology of antibiotic resistance. Int. J. Antimicrob. Agents **32**(Suppl 1):S2–S9. http://dx.doi.org/10.1016/j.ijantimicag.2008.06.016.
2. **Ruiz N, Kahne D, Silhavy TJ.** 2006. Advances in understanding bacterial outer-membrane biogenesis. Nat. Rev. Microbiol. **4**:57–66. http://dx.doi.org/10.1038/nrmicro1322.
3. **Leverrier P, Vertommen D, Collet JF.** 2010. Contribution of proteomics toward solving the fascinating mysteries of the biogenesis of the envelope of *Escherichia coli*. Proteomics **10**:771–784. http://dx.doi.org/10.1002/pmic.200900461.
4. **Van Wielink JE, Duine JA.** 1990. How big is the periplasmic space? Trends Biochem. Sci. **15**:136–137. http://dx.doi.org/10.1016/0968-0004(90)90208-S.
5. **Knowles TJ, Scott-Tucker A, Overduin M, Henderson IR.** 2009. Membrane protein architects: the role of the BAM complex in outer membrane protein assembly. Nat. Rev. Microbiol. **7**:206–214. http://dx.doi.org/10.1038/nrmicro2069.
6. **Ricci DP, Silhavy TJ.** 2012. The Bam machine: a molecular cooper. Biochim. Biophys. Acta **1818**:1067–1084. http://dx.doi.org/10.1016/j.bbamem.2011.08.020.
7. **Ruiz N, Kahne D, Silhavy TJ.** 2009. Transport of lipopolysaccharide across the cell envelope: the long road of discovery. Nat. Rev. Microbiol. **7**:677–683. http://dx.doi.org/10.1038/nrmicro2184.
8. **Rigel NW, Silhavy TJ.** 2012. Making a beta-barrel: assembly of outer membrane proteins in Gram-negative bacteria. Curr. Opin. Microbiol. **15**:189–193. http://dx.doi.org/10.1016/j.mib.2011.12.007.
9. **Ruiz N, Falcone B, Kahne D, Silhavy TJ.** 2005. Chemical conditionality: a genetic strategy to probe organelle assembly. Cell **121**:307–317. http://dx.doi.org/10.1016/j.cell.2005.02.014.
10. **Baba T, Ara T, Hasegawa M, Takai Y, Okumura Y, Baba M, Datsenko KA, Tomita M, Wanner BL, Mori H.** 2006. Construction of *Escherichia*

coli K-12 in-frame, single-gene knockout mutants: the Keio collection. Mol. Syst. Biol. **2:**2006.0008. http://dx.doi.org/10.1038/msb4100050.
11. **Nonaka G, Blankschien M, Herman C, Gross CA, Rhodius VA.** 2006. Regulon and promoter analysis of the *E. coli* heat-shock factor, σ^{32}, reveals a multifaceted cellular response to heat stress. Genes Dev. **20:**1776–1789. http://dx.doi.org/10.1101/gad.1428206.
12. **Uehara T, Parzych KR, Dinh T, Bernhardt TG.** 2010. Daughter cell separation is controlled by cytokinetic ring-activated cell wall hydrolysis. EMBO J. **29:**1412–1422. http://dx.doi.org/10.1038/emboj.2010.36.
13. **Bremer E, Silhavy TJ, Weisemann JM, Weinstock GM.** 1984. Lambda placMu: a transposable derivative of bacteriophage lambda for creating *lacZ* protein fusions in a single step. J. Bacteriol. **158:**1084–1093.
14. **Cherepanov PP, Wackernagel W.** 1995. Gene disruption in *Escherichia coli*: Tc^R and Km^R cassettes with the option of Flp-catalyzed excision of the antibiotic-resistance determinant. Gene **158:**9–14. http://dx.doi.org/10.1016/0378-1119(95)00193-A.
15. **Laemmli UK.** 1970. Cleavage of structural proteins during the assembly of the head of bacteriophage T4. Nature **227:**680–685. http://dx.doi.org/10.1038/227680a0.
16. **Collet JF, D'Souza JC, Jakob U, Bardwell JC.** 2003. Thioredoxin 2, an oxidative stress-induced protein, contains a high affinity zinc binding site. J. Biol. Chem. **278:**45325–45332. http://dx.doi.org/10.1074/jbc.M307818200.
17. **Jakob U, Eser M, Bardwell JC.** 2000. Redox switch of hsp33 has a novel zinc-binding motif. J. Biol. Chem. **275:**38302–38310. http://dx.doi.org/10.1074/jbc.M005957200.
18. **Beinert H.** 1983. Semi-micro methods for analysis of labile sulfide and of labile sulfide plus sulfane sulfur in unusually stable iron-sulfur proteins. Anal. Biochem. **131:**373–378. http://dx.doi.org/10.1016/0003-2697(83)90186-0.
19. **Sliusarenko O, Heinritz J, Emonet T, Jacobs-Wagner C.** 2011. High-throughput, subpixel precision analysis of bacterial morphogenesis and intracellular spatio-temporal dynamics. Mol. Microbiol. **80:**612–627. http://dx.doi.org/10.1111/j.1365-2958.2011.07579.x.
20. **Raetz CR, Whitfield C.** 2002. Lipopolysaccharide endotoxins. Annu. Rev. Biochem. **71:**635–700. http://dx.doi.org/10.1146/annurev.biochem.71.110601.135414.
21. **Hagan CL, Silhavy TJ, Kahne D.** 2011. beta-Barrel membrane protein assembly by the Bam complex. Annu. Rev. Biochem. **80:**189–210. http://dx.doi.org/10.1146/annurev-biochem-061408-144611.
22. **Narita S, Masui C, Suzuki T, Dohmae N, Akiyama Y.** 2013. Protease homolog BepA (YfgC) promotes assembly and degradation of beta-barrel membrane proteins in *Escherichia coli*. Proc. Natl. Acad. Sci. U. S. A. **110:**E3612–3621. http://dx.doi.org/10.1073/pnas.1312012110.
23. **Casadaban MJ, Cohen SN.** 1980. Analysis of gene control signals by DNA fusion and cloning in *Escherichia coli*. J. Mol. Biol. **138:**179–207. http://dx.doi.org/10.1016/0022-2836(80)90283-1.
24. **Casadaban MJ.** 1976. Transposition and fusion of the lac genes to selected promoters in *Escherichia coli* using bacteriophage lambda and Mu. J. Mol. Biol. **104:**541–555. http://dx.doi.org/10.1016/0022-2836(76)90119-4.
25. **Cho BK, Zengler K, Qiu Y, Park YS, Knight EM, Barrett CL, Gao Y, Palsson BO.** 2009. The transcription unit architecture of the *Escherichia coli* genome. Nat. Biotechnol. **27:**1043–1049. http://dx.doi.org/10.1038/nbt.1582.
26. **Daley DO, Rapp M, Granseth E, Melen K, Drew D, von Heijne G.** 2005. Global topology analysis of the *Escherichia coli* inner membrane proteome. Science **308:**1321–1323. http://dx.doi.org/10.1126/science.1109730.
27. **Nielsen H, Engelbrecht J, Brunak S, von Heijne G.** 1997. A neural network method for identification of prokaryotic and eukaryotic signal peptides and prediction of their cleavage sites. Int. J. Neural Syst. **8:**581–599. http://dx.doi.org/10.1142/S0129065797000537.
28. **von Heijne G, Gavel Y.** 1988. Topogenic signals in integral membrane proteins. Eur. J. Biochem. **174:**671–678. http://dx.doi.org/10.1111/j.1432-1033.1988.tb14150.x.
29. **Beam CE, Saveson CJ, Lovett ST.** 2002. Role for *radA*/*sms* in recombination intermediate processing in *Escherichia coli*. J. Bacteriol. **184:**6836–6844. http://dx.doi.org/10.1128/JB.184.24.6836-6844.2002.
30. **Lovenberg W, Sobel BE.** 1965. Rubredoxin: a new electron transfer protein from *Clostridium pasteurianum*. Proc. Natl. Acad. Sci. U. S. A. **54:**193–199. http://dx.doi.org/10.1073/pnas.54.1.193.
31. **Lee HJ, Lian LY, Scrutton NS.** 1997. Recombinant two-iron rubredoxin of *Pseudomonas oleovorans*: overexpression, purification and characterization by optical, CD and 113Cd NMR spectroscopies. Biochem. J. **328:**131–136.
32. **Zheng P, Takayama SJ, Mauk AG, Li H.** 2012. Hydrogen bond strength modulates the mechanical strength of ferric-thiolate bonds in rubredoxin. J. Am. Chem. Soc. **134:**4124–4131. http://dx.doi.org/10.1021/ja2078812.
33. **Blatch GL, Lassle M.** 1999. The tetratricopeptide repeat: a structural motif mediating protein-protein interactions. Bioessays **21:**932–939. http://dx.doi.org/10.1002/(SICI)1521-1878(199911)21:11<932::AID-BIES5>3.0.CO;2-N.
34. **Liu J, Oganesyan N, Shin DH, Jancarik J, Yokota H, Kim R, Kim SH.** 2005. Structural characterization of an iron-sulfur cluster assembly protein IscU in a zinc-bound form. Proteins **59:**875–881. http://dx.doi.org/10.1002/prot.20421.
35. **Zhang J, Kasciukovic T, White MF.** 2012. The CRISPR associated protein Cas4 is a 5′ to 3′ DNA exonuclease with an iron-sulfur cluster. PLoS One **7:**e47232. http://dx.doi.org/10.1371/journal.pone.0047232.
36. **Ramelot TA, Cort JR, Goldsmith-Fischman S, Kornhaber GJ, Xiao R, Shastry R, Acton TB, Honig B, Montelione GT, Kennedy MA.** 2004. Solution NMR structure of the iron-sulfur cluster assembly protein U (IscU) with zinc bound at the active site. J. Mol. Biol. **344:**567–583. http://dx.doi.org/10.1016/j.jmb.2004.08.038.
37. **Huang KC, Mukhopadhyay R, Wen B, Gitai Z, Wingreen NS.** 2008. Cell shape and cell-wall organization in Gram-negative bacteria. Proc. Natl. Acad. Sci. U. S. A. **105:**19282–19287. http://dx.doi.org/10.1073/pnas.0805309105.
38. **Burdett ID, Murray RG.** 1974. Septum formation in *Escherichia coli*: characterization of septal structure and the effects of antibiotics on cell division. J. Bacteriol. **119:**303–324.
39. **Meisel U, Holtje JV, Vollmer W.** 2003. Overproduction of inactive variants of the murein synthase PBP1B causes lysis in *Escherichia coli*. J. Bacteriol. **185:**5342–5348. http://dx.doi.org/10.1128/JB.185.18.5342-5348.2003.
40. **Yao Z, Kahne D, Kishony R.** 2012. Distinct single-cell morphological dynamics under beta-lactam antibiotics. Mol. Cell **48:**705–712. http://dx.doi.org/10.1016/j.molcel.2012.09.016.
41. **Hara H, Yamamoto Y, Higashitani A, Suzuki H, Nishimura Y.** 1991. Cloning, mapping, and characterization of the *Escherichia coli prc* gene, which is involved in C-terminal processing of penicillin-binding protein 3. J. Bacteriol. **173:**4799–4813.
42. **Ohara M, Wu HC, Sankaran K, Rick PD.** 1999. Identification and characterization of a new lipoprotein, NlpI, in *Escherichia coli* K-12. J. Bacteriol. **181:**4318–4325.
43. **Schmidt KL, Peterson ND, Kustusch RJ, Wissel MC, Graham B, Phillips GJ, Weiss DS.** 2004. A predicted ABC transporter, FtsEX, is needed for cell division in *Escherichia coli*. J. Bacteriol. **186:**785–793. http://dx.doi.org/10.1128/JB.186.3.785-793.2004.
44. **Bernhardt TG, de Boer PA.** 2004. Screening for synthetic lethal mutants in *Escherichia coli* and identification of EnvC (YibP) as a periplasmic septal ring factor with murein hydrolase activity. Mol. Microbiol. **52:**1255–1269. http://dx.doi.org/10.1111/j.1365-2958.2004.04063.x.
45. **Peters NT, Morlot C, Yang DC, Uehara T, Vernet T, Bernhardt TG.** 2013. Structure-function analysis of the LytM domain of EnvC, an activator of cell wall remodelling at the *Escherichia coli* division site. Mol. Microbiol. **89:**690–701. http://dx.doi.org/10.1111/mmi.12304.
46. **Tamae C, Liu A, Kim K, Sitz D, Hong J, Becket E, Bui A, Solaimani P, Tran KP, Yang H, Miller JH.** 2008. Determination of antibiotic hypersensitivity among 4,000 single-gene-knockout mutants of *Escherichia coli*. J. Bacteriol. **190:**5981–5988. http://dx.doi.org/10.1128/JB.01982-07.
47. **Braun V, Sieglin U.** 1970. The covalent murein-lipoprotein structure of the *Escherichia coli* cell wall. The attachment site of the lipoprotein on the murein. Eur. J. Biochem. **13:**336–346.
48. **Braun V, Wolff H.** 1970. The murein-lipoprotein linkage in the cell wall of *Escherichia coli*. Eur. J. Biochem. **14:**387–391. http://dx.doi.org/10.1111/j.1432-1033.1970.tb00301.x.
49. **Paradis-Bleau C, Markovski M, Uehara T, Lupoli TJ, Walker S, Kahne DE, Bernhardt TG.** 2010. Lipoprotein cofactors located in the outer membrane activate bacterial cell wall polymerases. Cell **143:**1110–1120. http://dx.doi.org/10.1016/j.cell.2010.11.037.
50. **Typas A, Banzhaf M, van den Berg van Saparoea B, Verheul J, Biboy J, Nichols RJ, Zietek M, Beilharz K, Kannenberg K, von Rechenberg M, Breukink E, den Blaauwen T, Gross CA, Vollmer W.** 2010. Regulation of peptidoglycan synthesis by outer-membrane proteins. Cell **143:**1097–1109. http://dx.doi.org/10.1016/j.cell.2010.11.038.